Article

Cell Reports

Streptococcus pneumoniae Infection Promotes Histone H3 Dephosphorylation by Modulating Host PP1 Phosphatase

Graphical Abstract

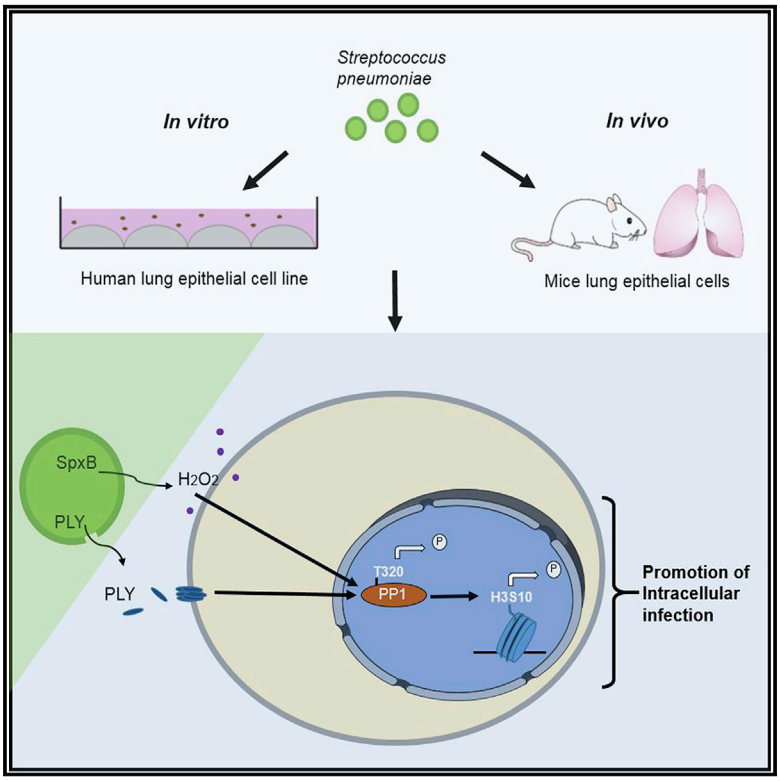

Authors

Wenyang Dong, Orhan Rasid, Christine Chevalier, Michael Connor, Matthew J.G. Eldridge, Melanie Anne Hamon

Correspondence

melanie.hamon@pasteur.fr

In Brief

Dong et al. show that *Streptococcus pneumoniae* infection induces histone H3 dephosphorylation in lung epithelial cells, through two bacterial factors, PLY and SpxB. Infection-triggered activation of the host phosphatase PP1 is required for this histone modification and efficient intracellular infection.

Highlights

- *Streptococcus pneumoniae* infection induces dephosphorylation of histone H3
- The bacterial factors PLY and SpxB contribute to H3S10 dephosphorylation
- Host PP1 mediates H3S10 dephosphorylation and is important for intracellular infection
- PP1 is activated upon *S. pneumoniae* infection through T320 dephosphorylation

Dong et al., 2020, Cell Reports *30*, 4016–4026
March 24, 2020
https://doi.org/10.1016/j.celrep.2020.02.116

CellPress

OPEN ACCESS
CellPress

Cell Reports
Article

Streptococcus pneumoniae Infection Promotes Histone H3 Dephosphorylation by Modulating Host PP1 Phosphatase

Wenyang Dong,[1,2] Orhan Rasid,[1] Christine Chevalier,[1] Michael Connor,[1] Matthew J.G. Eldridge,[1] and Melanie Anne Hamon[1,3,*]
[1]G5 Chromatine et Infection, Institut Pasteur, Paris 75015, France
[2]Université de Paris, Sorbonne Paris Cité, Paris, France
[3]Lead Contact
*Correspondence: melanie.hamon@pasteur.fr
https://doi.org/10.1016/j.celrep.2020.02.116

SUMMARY

Pathogenic bacteria can alter host gene expression through post-translational modifications of histones. We show that a natural colonizer, *Streptococcus pneumoniae*, induces specific histone modifications, including robust dephosphorylation of histone H3 on serine 10 (H3S10), during infection of respiratory epithelial cells. The bacterial pore-forming toxin pneumolysin (PLY), along with the pyruvate oxidase SpxB responsible for H_2O_2 production, play important roles in the induction of this modification. The combined effects of PLY and H_2O_2 trigger host signaling that culminates in H3S10 dephosphorylation, which is mediated by the host cell phosphatase PP1. Strikingly, *S. pneumoniae* infection induces dephosphorylation and subsequent activation of PP1 catalytic activity. Colonization of PP1 catalytically deficient cells results in impaired intracellular *S. pneumoniae* survival and infection. Interestingly, PP1 activation and H3S10 dephosphorylation are not restricted to *S. pneumoniae* and appear to be general epigenomic mechanisms favoring intracellular survival of pathogenic bacteria.

INTRODUCTION

Streptococcus pneumoniae is a Gram-positive, extracellular bacterium, which colonizes the human nasopharynx and respiratory tract. It is a leading cause of bacterial pneumonia and meningitis worldwide, particularly in developing nations (Wahl et al., 2018). In the complex relationship with its host, *S. pneumoniae* can act as both an adapted commensal and an invasive pathogen. On the one hand, *S. pneumoniae* may reside asymptomatically in the upper respiratory tract, a phenomenon that is particularly common in children and greatly contributes to transmission. On the other hand, bacteria can cause pneumonia or breach epithelial barriers, enter the bloodstream, and eventually cause severe invasive pneumococcal diseases (IPDs), such as meningitis, and sepsis. To date, 98 serotypes of this encapsulated diplococcus have been described, based on variations in their capsule polysaccharide (CPS) (Kadioglu et al., 2008). However, not all serotypes are equal in their capacity to cause IPDs; only 20–30 of them are principally associated with invasiveness diseases, such as serotypes 1, 4, and 14 (Geno et al., 2015; Mehr and Wood, 2012). In contrast, several serotypes, such as 6B, 11A, and 23F, are more likely to be carried for longer periods and are thus regarded as carriage serotypes (Geno et al., 2015). However, because of the introduction of pneumococcal conjugate vaccines and prominent capsule switching, the serotype prevalence and distribution in IPDs and carriage serotypes regularly change.

For both carriage and invasive pneumococcal strains, the establishment of colonization begins upon contact with the host respiratory epithelium. *S. pneumoniae* interacts with epithelial cells via multiple and complex processes, and this multifactorial event has been well characterized with respect the bacterial factors involved. Surface factors, such as CbpA and ChoP, have been reported to participate in adhesion to epithelial cells (Kadioglu et al., 2008). Another major virulence factor, the pore-forming toxin pneumolysin (PLY) is proposed to be involved in invasion by breaching the epithelium (Weiser et al., 2018). However, the processes involved in pneumococcal-epithelial interactions, such as how *S. pneumoniae* modulates host-cell signaling, are understudied.

Recent studies show that pathogens reprogram host cells during infection through bacteria-triggered histone modifications, which modulate host transcription (Bierne et al., 2012). In eukaryotic cells, DNA is packaged with histones into chromatin, and the covalent post-translational modifications at the tails of the core histones function to dynamically control DNA accessibility, affect the recruitment and stabilization of transcription-associated factors, and therefore, regulate the cell's transcriptional programs (Hamon and Cossart, 2008). Bacterial pathogens have been shown to target host histones directly, through the secretion of factors targeting chromatin and named nucleomodulins, or indirectly, through modulation of host signaling cascades. However, histone modifications induced by a natural colonizer, such as *S. pneumoniae*, have not yet, to our knowledge, been explored.

During bacterial infection, histone H3 was found to be dephosphorylated after the loss of membrane integrity mediated either by the secretion of cholesterol-dependent cytolysin (CDC) toxin

or by insertion of translocon from the type III secretion system (Dortet et al., 2018; Hamon et al., 2007). H3 dephosphorylation on serine 10 (H3S10) was shown to be induced *in vitro* in epithelial cells and to correlate with the repression of inflammatory genes. Although cellular processes, such as entry into mitosis or activation by extracellular signals (EGF, cellular stress, or inflammation) have been shown to be associated with H3S10 phosphorylation, the role of this modification in these processes is not fully understood (Mahadevan et al., 1991; Saccani et al., 2002; Sawicka et al., 2014). Key kinase signaling pathways, including mitogen-activated protein kinase (MAPK) and nuclear factor κB (NF-κB), induce the phosphorylation of histone H3 on residue 10 (H3S10) or 28 (H3S28), which are important for crosstalk with histone H3 acetylation, a canonical mark of transcriptional activation (Drobic et al., 2010; Yamamoto et al., 2003). In contrast, how H3S10 becomes dephosphorylated is less well understood. Furthermore, the molecular basis and the role of this histone modification during bacterial infection remain unknown.

In this article, we reveal that *S. pneumoniae* induces histone modifications in host lung epithelial cells, both *in vitro* and *in vivo*. We identify the CDC toxin PLY as a key factor in mediating H3 dephosphorylation but also reveal the strong contribution of the pyruvate oxidase, SpxB. Both PLY and SpxB factors activate the host phosphatase PP1, which we show is responsible for H3 dephosphorylation. Interestingly, we find that infection triggers dephosphorylation of PP1 on threonine 320 (T320), which is required for its activation, and that this process is necessary to permit efficient intracellular infection. By describing the molecular basis and the role of H3S10 dephosphorylation, we illustrate a common mechanism of host alteration by bacteria relevant during both colonization and infection.

RESULTS

Streptococcus pneumoniae Induces Dephosphorylation of Histone H3 on Serine 10 during Infection

Histone H3 dephosphorylation on serine 10 was initially observed after treatment of epithelial cells with purified bacterial toxins, including PLY of *S. pneumoniae* (Hamon et al., 2007). To evaluate whether histone H3 phosphorylation is modulated by bacteria during infection, we exposed A549 lung epithelial cells to two different strains of *S. pneumoniae* (R6 and TIGR4) at increasing multiplicities of infection (MOIs) and assessed the phosphorylation of H3S10 by immunoblotting. As a control, the total levels of H3 and actin were also measured. Data in Figure 1A show that H3S10 is strongly dephosphorylated, and the effect is proportional to the number of bacteria used in the infection. We further validated that this effect was not restricted only to alveolar epithelial A549 cells because bronchial epithelial Beas-2B cells displayed the same reduction in phosphorylation of histone H3 at serine 10 (H3S10ph) levels (Figure S1A). H3T3, H3T11, and H3S28 were also dephosphorylated in response to bacteria; however, H3T6 was not, suggesting only specific residues are targeted (Figure S1B). Because H3S10ph has been previously associated with bacterial infection (Arbibe et al., 2007; Hamon et al., 2007; Saccani et al., 2002), we focused our study on this modification.

Given that H3S10 dephosphorylation was observed during infection with two different laboratory strains, we hypothesized that this effect was a shared mechanism among *S. pneumonia* serotypes. We assessed clonal representatives of different invasive and carriage serotypes for their ability to induce H3S10 dephosphorylation. We show that all serotypes tested induced strong H3S10 dephosphorylation in A549 cells (Figure 1B). These results demonstrate that reduction of H3S10ph levels is a common feature of *S. pneumoniae* infection and is induced by clinical isolates as well as laboratory strains.

H3S10ph has been associated with the mitotic phase of the cell cycle (Sawicka and Seiser, 2012); therefore, we investigated whether the observed loss reflected changes in the cell cycle induced by infection. Cells were synchronized with thymidine, infected upon release, and the proportion of cells in each stage of the cell cycle was measured using propidium iodine staining. Fluorescence-activated cell sorting (FACS) analysis showed no significant difference in the percentage of cells in each stage between uninfected and infected cells (Figure S1C), strongly suggesting that infection does not affect the cell cycle. Furthermore, immunofluorescence experiments were performed to determine H3S10ph levels in non-mitotic cells. Nuclear staining with DAPI clearly distinguishes cells in interphase versus mitosis and allows direct visualization of interphase cells, confirming that many cells which do not have condensed chromosomes stain positive for H3S10ph (Figure 1C). Quantification of fluorescence intensity upon infection with *S. pneumoniae* shows a significant reduction compared with uninfected cells (Figure 1C). These data further support the finding that infection-induced dephosphorylation occurs in interphase cells, independent of the cell cycle.

We next determined whether H3S10 dephosphorylation occurred during *in vivo* infection. We performed intranasal inoculation of mice with *S. pneumoniae* and used antibodies against cell lineage markers to specific cell types isolated from collected mouse lungs (Figure S1D). The levels of H3S10 phosphorylation in epithelial cells after 24 h of infection were further evaluated by FACS analysis. In comparing infected to uninfected cells, a shift in the fluorescence level of a large proportion of epithelial cells was observed (Figure 1D). Interestingly, dephosphorylation was mainly detected in epithelial cells, and other monitored cells did not display significant changes in this histone mark (Figure S1E). These data further support that H3 dephosphorylation occurs in terminally differentiated cells, independent of the cell cycle. Therefore, *S. pneumoniae* induces specific H3S10 dephosphorylation in epithelial cells during infection.

S. Pneumoniae Toxin PLY Is Important for H3S10 Dephosphorylation

The cholesterol-dependent cytolysin of *S. pneumoniae*, PLY, was previously shown to induce H3S10 dephosphorylation when treating epithelial cells with purified toxin (Hamon et al., 2007). We thus hypothesized that PLY was the main factor responsible for this modification during infection. Chromosomal deletion mutants of PLY were generated in both R6 and TIGR4 strains of *S. pneumoniae* and were tested for their ability to dephosphorylate H3. Immunoblotting experiments show that H3 dephosphorylation was only partially blocked with the Δ*ply*

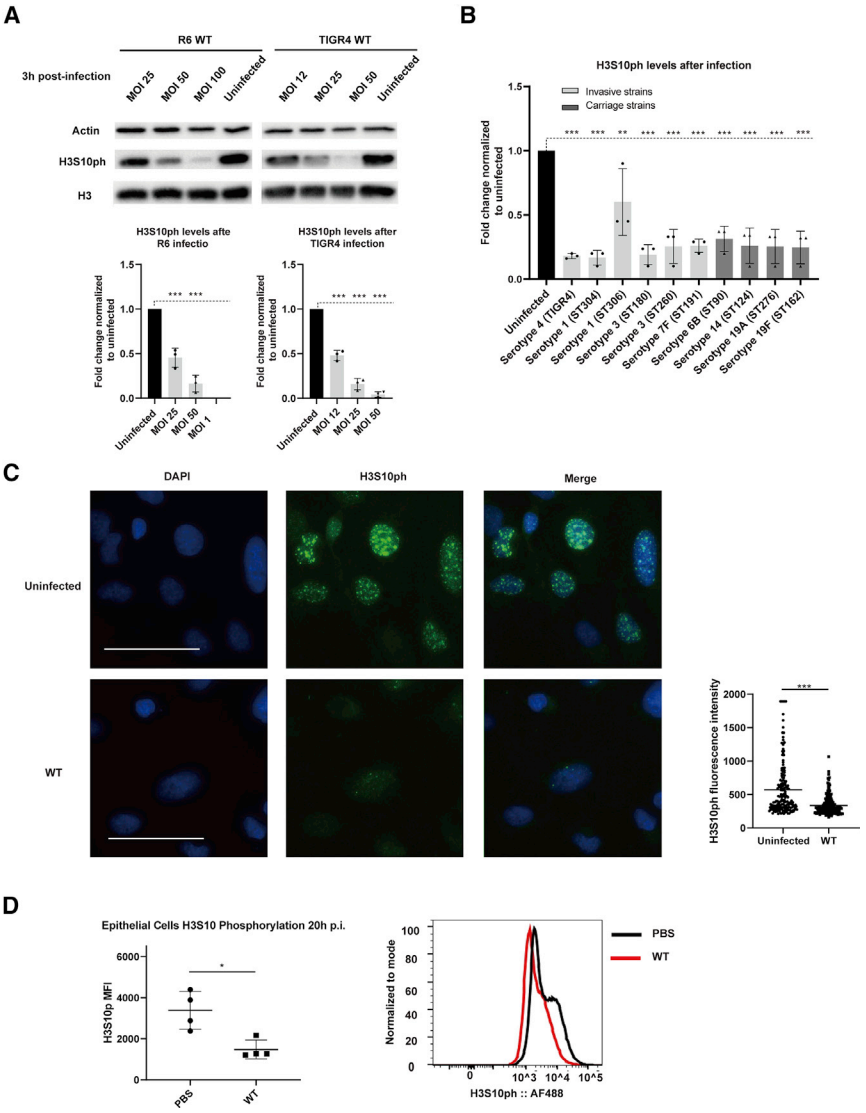

Figure 1. *Streptococcus pneumoniae* Induces Specific Dephosphorylation of Histone H3 on Serine 10 Independently of the Cell Cycle

(A) Phosphorylation levels of histone H3S10, as detected by immunoblotting in uninfected A549 cells and cells infected with *S. pneumonia* strain R6 or TIGR4, at the indicated multiplicities of infection (MOIs). Quantification of H3S10ph immunoblots were normalized first to total actin levels and then to the uninfected sample. Error bars represent SD of three independent experiments. Statistical significance was calculated by the one-way ANOVA method (Dunnett's post hoc test, uninfected as control group). ***$p < 0.001$.

(B) Quantification of levels of H3S10 phosphorylation detected by immunoblotting in uninfected A549 cells and cells infected with TIGR4 or clinical *S. pneumonia* strains (from carriage or invasiveness); serotypes and MLST types at MOI 25 are indicated. Error bars represent SD of three independent experiments. Statistical significance was calculated using one-way ANOVA method (Dunnett's post hoc test, uninfected as the control group). **$p < 0.01$, ***$p < 0.001$.

(C) H3S10ph was detected by immunofluorescence in Beas-2B cells under uninfected and 1-h TIGR4 (MOI = 25)-infected conditions. Size bars represent 50 μm. On the right, the quantification of nuclear fluorescence intensity integrates independent duplicate experiments ($n \geq 200$ cells per condition). Statistical significance was calculated using a Student's t test. ***$p < 0.001$.

(D) H3S10ph levels of lung epithelial cells from mice treated with PBS or infected with *S. pneumonia* TIGR4 (5×10^6 colony-forming units [CFUs]) for 20 h were analyzed by FACS. Mean fluorescence intensity (MFI) is represented with error bars indicating SD. n = 4 mice per condition. Statistical significance was calculated using a Student's t test. *$p < 0.05$.

See also Figure S1.

mutant as compared with wild-type (WT) infection (Figure 2A). Because PLY does not have a signal sequence for secretion, it is thought that the toxin is release upon lysis of bacteria in a manner dependent upon the autolysin LytA. We, therefore, generated a *lytA*-deletion mutant, which releases less PLY than WT bacteria and induces a similar dephosphorylation of H3 as a Δ*ply* mutant (Figures S2A and SB). Therefore, H3 dephosphorylation is in part mediated by PLY, which is released upon LytA-dependent lysis of a subpopulation of bacteria.

To understand how PLY was inducing histone modifications, we complemented the Δ*ply* mutant with a PLY bearing a point mutation, W436A, rendering it non-hemolytic (Malet et al., 2017). We compared the level of H3S10ph of the mutant to that of a strain complemented with WT PLY. The complemented WT induced the same level of H3S10 dephosphorylation as WT bacteria, whereas the W436A mutant phenocopied the Δ*ply* mutant (Figure 2B). Therefore, PLY contributes to dephosphorylation of H3 in a pore formation-dependent manner. Given that the level of H3S10ph was clearly not restored to uninfected levels upon infection with the Δ*ply* mutant, other additional contributing bacterial factors are probably also responsible for inducing this histone modification.

H_2O_2 Generated by SpxB Is Required for *S. pneumoniae*-Mediated H3S10 Dephosphorylation

Reports have shown that a stress response, such as oxidative stress, can lead to H3 dephosphorylation (Jeong et al., 2013; Shimada et al., 2010). Interestingly, *S. pneumoniae* expresses a pyruvate oxidase that converts pyruvate to acetyl-phosphate and generates H_2O_2 as a byproduct. The produced H_2O_2, which is freely diffusible across membranes, can be detected in the supernatant of infected cells, and a deletion of the SpxB oxidase results in a complete block of H_2O_2 production (Figure S3A). To determine whether SpxB was contributing to H3 dephosphorylation, we infected cells with a deletion mutant. In both strains

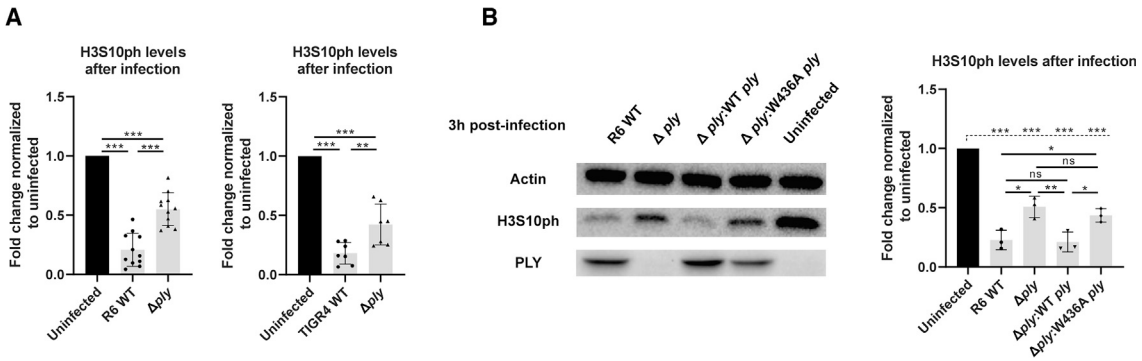

Figure 2. *S. pneumoniae* Toxin PLY Is Important for H3S10 Dephosphorylation

(A) Quantification of H3S10ph in uninfected cells, cells infected with WT *S. pneumonia* strains R6 (MOI = 50) and TIGR4 (MOI = 25) and their respective *Δply* mutant strains, for 3 h.

(B) Representative immunoblots of cells infected with WT *S. pneumonia* (R6 strain), a *Δply* mutant, a *Δply* mutant complemented with WT *ply*, or a *ply* point mutant without pore-forming activity (W436A) at MOI 50 for 3 h.

All quantifications in graphs show the means ± SD of at least three independent experiments. Statistical significance was calculated by one-way ANOVA method (Turkey post hoc test when compared within infection groups, as indicated with solid line, or Dunnett's post hoc test when compared with the uninfected control, as indicated with dotted line). *p < 0.05, **p < 0.01, ***p < 0.001.

See also Figure S2.

R6 and Tigr4, H3 dephosphorylation was prevented upon infection with a Δ*spxB* mutant. In fact, H3S10ph levels were comparable to the uninfected level upon infection with Δ*spxB* or a double Δ*ply*Δ*spxB* mutant (Figure 3A). Additionally, we performed immunofluorescence experiments with the double Δ*ply*Δ*spxB* mutant, and quantification of H3S10ph fluorescence intensity showed that the double mutant did not induce dephosphorylation (Figure 3B).

To determine whether *S. pneumoniae*-mediated H3 dephosphorylation requires the catalytic activity of SpxB and H_2O_2, the byproduct of catalysis, we generated a Δ*spxB* mutant complemented with WT *spxB* and/or a catalytically inactive *spxB* (*spxB* P449L) (Ramos-Montañez et al., 2008). Both strains were used in infection, and the levels of H3S10ph were determined by immunoblotting. Although Δ*spxB:spxB* was able to restore H3 dephosphorylation to WT levels, the catalytically inactive complement, Δ*spxB:spxBP449L*, did not (Figure 3D). To further show that it is the byproduct of SpxB catalysis, H_2O_2, rather than another metabolic intermediate, which is important for H3 dephosphorylation, we performed experiments in the presence of catalase. Catalase is an enzyme that converts H_2O_2 to water and oxygen and thereby neutralizes the downstream effects of H_2O_2. Cells infected with Δ*ply* TIGR4 or treated with infection supernatant displayed significant H3 dephosphorylation (Figures 3E and 3F). However, upon catalase treatment, H3 dephosphorylation was significantly impaired, reinforcing the finding that H_2O_2 produced by SpxB is the main driver for H3 dephosphorylation. In fact, H_2O_2 alone induces H3 dephosphorylation in A549 cells in a dose-dependent manner (Figure S3B). Therefore, H_2O_2 generated by SpxB is a factor contributing to H3 dephosphorylation in addition to the pore-forming toxin PLY.

In vivo experiments were performed to determine whether SpxB and PLY were necessary for H3 dephosphorylation in lung epithelial cells. Although WT infection led to a significant shift in phosphorylation H3 levels, the double Δ*ply*Δ*spxB* mutant did not. In fact, H3S10 dephosphorylation did not occur when inoculating mice intranasally with the Δ*ply*Δ*spxB* mutant (Figure 3C). Therefore, both PLY and SpxB are required to induce H3 dephosphorylation upon infection in both *in vitro* and *in vivo* epithelial cells. We noticed that a single *ΔspxB* mutant did not induce greater H3S10 dephosphorylation than a double Δ*ply*Δ*spxB* mutant. This could be explained by the finding that a mutant in SpxB is diminished in PLY release and pore-formation on epithelial cells (Bryant et al., 2016).

PP1 Is the Host Phosphatase Mediating H3S10 Dephosphorylation

Given that neither PLY nor SpxB directly target H3S10 for modification, we searched for a host phosphatase that could mediate the observed dephosphorylation. We first used chemical inhibitors that target known phosphatases: okadaic acid, a potent and selective inhibitor of protein phosphatase 1 (PP1) and 2A (PP2A), with a greater potency for 2A, and tautomycetin, which specifically inhibits PP1. Cells were pretreated with the two inhibitors and subsequently infected with either R6 or TIGR4 strains of *S. pneumoniae*. Detection of phosphorylated H3 levels by immunoblotting show that okadaic acid had no effect, whereas tautomycetin blocked infection-induced dephosphorylation (Figures 4A and S4A). These results were further validated by RNA interference using small interfering RNA (siRNA) targeting all isoforms of PP1 (α, β, and γ). The knockdown efficiency siRNA clearly showed that the level of all isoforms was equally decreased (Figure S4B). Under those conditions, H3S10 dephosphorylation was fully blocked upon infection, similar to the results obtained with tautomycetin (Figure 4B). Consistent with PP1 being the main phosphatase targeting H3, siRNA of PP1 also fully blocked H_2O_2 and purified PLY-mediated H3 dephosphorylation

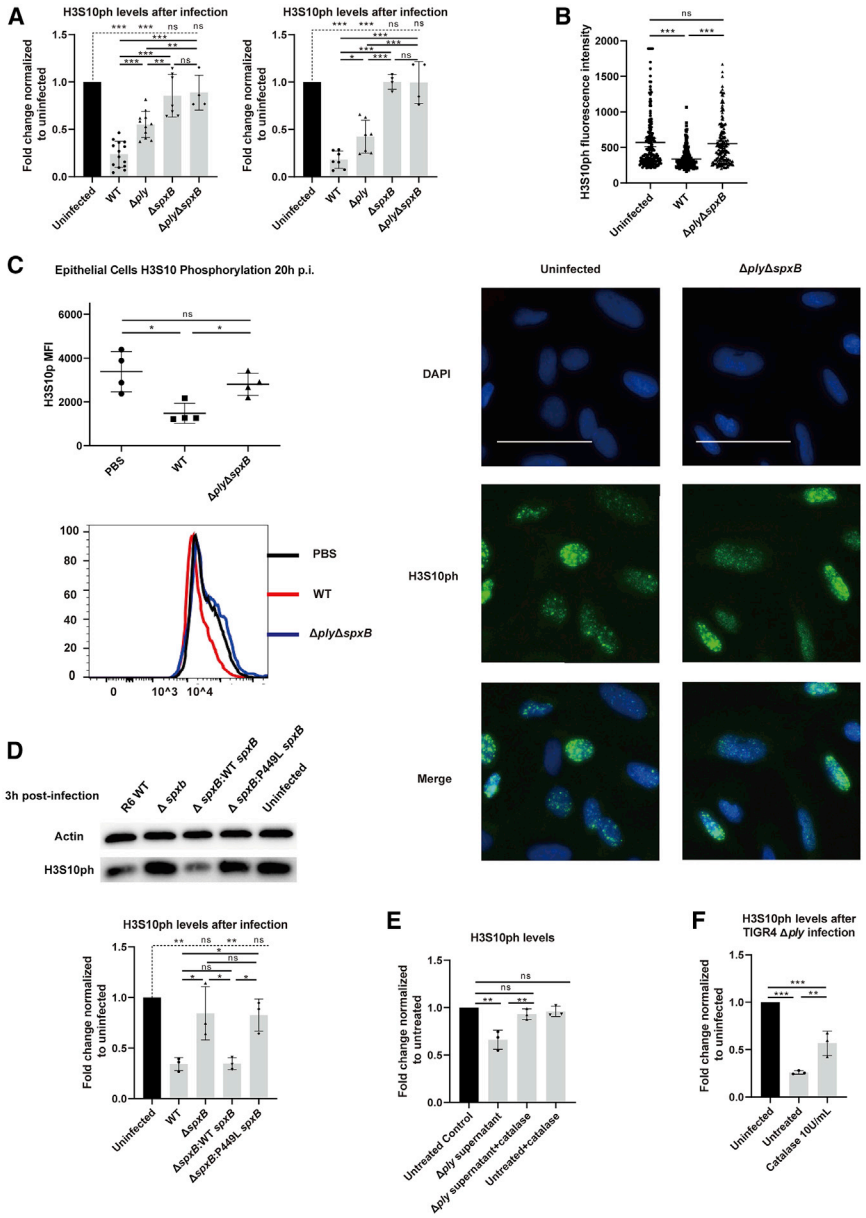

Figure 3. H_2O_2 Generated by SpxB Is Required for *S. pneumoniae*-Mediated H3S10 Dephosphorylation

(A) Quantification of H3S10ph in uninfected cells, cells infected with WT *S. pneumonia* strains R6 (MOI = 50) and TIGR4 (MOI = 25), a *Δply* mutant, a *ΔspxB* mutant, or a *ΔplyΔspxB* double mutant for 3 h.

(B) H3S10ph was detected by immunofluorescence in Beas-2B cells under uninfected and 1h (MOI = 25) infected conditions. On the right, the quantification of nuclear fluorescence intensity integrates independent duplicate experiments (n ≥ 200 cells per condition). Size bars represent 50 μm.

(C) H3S10ph levels of lung epithelial cells from mice treated with PBS, WT *S. pneumonia* TIGR4 (5 × 10^6 CFU), or a *ΔplyΔspxB* double mutant (5 × 10^6 CFU) for 20 h were analyzed by FACS. Mean fluorescence intensity (MFI) is represented with error bars indicating SD, n = 4 mice per condition.

(D) Immunoblot images are shown on the left and quantifications on the right. The left image is shown for representative immunoblots of cells infected with WT *S. pneumonia* (R6 strain), a *ΔspxB* mutant, a *ΔspxB* mutant complemented with WT *spxB*, or a *spxB* point mutant without catalytic activity (P449L) at MOI = 50 for 3 h.

(E) Cells were incubated 2h with the filter-sterilized supernatant from infection wells, or with 15 min catalase pretreated filter-sterilized supernatant, or 15 min catalase pretreated cell culture medium, respectively.

(F) Quantification of H3S10ph in uninfected cells, cells infected with TIGR4 *ply* mutant (with or without catalase during infection) at MOI = 25 for 3 h.

Error bars in the quantifications represent SD of at least three independent experiments. Statistical significance was calculated by one-way ANOVA method (Turkey post hoc test when compared within infection groups, as indicated with the solid line, or Dunnett's post hoc test when compared with uninfected control, as indicated with the dotted line). *p < 0.05, **p < 0.01, ***p < 0.001. See also Figure S3.

(Figures 4B–4D). Together these results show that PP1 is the phosphatase involved in dephosphorylating H3 and that both PLY and SpxB mediate this effect through the same host pathway.

Previous studies have demonstrated that other toxins of the CDC family, such as listeriolysin O (LLO) from *Listeria monocytogenes*, also induced dephosphorylation of H3S10, but they did not identify the mechanism at play (Hamon et al., 2007). Therefore, we tested whether PP1 was also required for LLO-induced H3 dephosphorylation. Cells were treated with purified LLO, and H3 dephosphorylation was observed in HeLa cells (Figures 4E and 4F). However, upon pretreating cells with tautomycetin or by silencing the expression PP1 with siRNA, H3 dephosphorylation was blocked (Figures 4E and 4F). Therefore, PP1 is modulated by at least two bacterial toxins mediating H3S10 dephosphorylation.

Bacterial Infection Induces Dephosphorylation of PP1

In its resting state, PP1 is phosphorylated on T320, and dephosphorylation of this residue correlates with PP1 activation. Therefore, we determined whether PP1 was being activated by infection through dephosphorylation of T320 (Hou et al., 2013). First, lysates from infected and non-infected cells were probed by immunoblotting for the total levels of each PP1 isoform (Figure 5A). Importantly, the total level of PP1 was unaltered by infection, regardless of the mutant used. In contrast, the level of phosphorylated PP1 was significantly decreased upon infection with WT *S. pneumoniae* (TIGR4). Interestingly, PP1

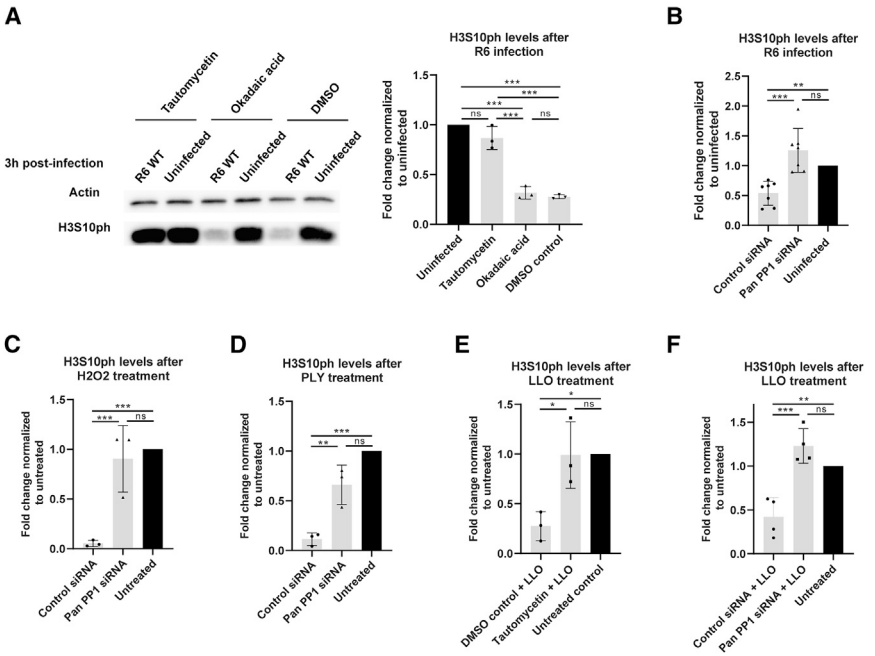

Figure 4. PP1 Is the Host Phosphatase Mediating H3S10 Dephosphorylation

(A) Representative immunoblot images are shown on the left and quantifications on the right. A549 cells pretreated with the PP1 inhibitor Tautomycetin, the PP2A inhibitor okadaic acid, or DMSO as the control and infected with R6 (MOI = 50) for 3 h.

(B) A549 cells are transfected with PP1 siRNA or control siRNA before 3 h R6 (MOI = 50) infection.

(C) A549 cells are transfected with PP1 siRNA or control siRNA before PLY treatment for 30 min.

(D) A549 cells are transfected with PP1 siRNA or control siRNA before H_2O_2 treatment for 1 h.

(E) HeLa cells are pretreated with PP1 inhibitor Tautomycetin before LLO treatment for 20 min.

(F) HeLa cells are transfected with PP1 siRNA or control siRNA before LLO treatment for 20 min.

All quantification graphs are of at least three independent experiments. All quantifications in graphs show the means ± SD, and statistical significance was calculated by one-way ANOVA method (Turkey post hoc test). **p < 0.01, ***p < 0.001.

See also Figure S4.

dephosphorylation was partially rescued upon infection with a Δ*ply* mutant and as fully prevented upon infection with a Δ*spxB* or the double Δ*ply*Δ*spxB* mutant. Therefore, the levels of phosphorylated PP1 fully correlated with the levels of phosphorylated H3S10 (Figure 5B), strongly suggesting that activation of PP1 by dephosphorylation led to dephosphorylation of H3.

We confirmed this finding by immunofluorescence by evaluating the level of phosphorylated PP1 in A549 cells. Interestingly, PP1 became dephosphorylated specifically in the nucleus of cells infected with WT bacteria (TIGR4), where histone H3 dephosphorylation occurs (Figure 5C). In contrast, the levels of nuclear phosphorylated PP1 did not change upon infection with the double Δ*ply*Δ*spxB* mutant. Because tautomycetin blocked infection-induced H3 dephosphorylation, we measured the corresponding levels of phosphorylated PP1. Tautomycetin fully blocked infection-induced PP1 dephosphorylation and appeared to induce phosphorylation (Figures 5C and S5A). These results show that the effect of PLY and SpxB converge on PP1, which likely auto-dephosphorylates itself.

Our data show that other toxins in the CDC family, such as LLO, mediate H3 dephosphorylation through PP1. We, therefore, wanted to determine whether infection with *Listeria monocytogenes*, which produces LLO, also induced PP1 T320 dephosphorylation. To address this point, we infected HeLa cells with either WT *L. monocytogenes* or a mutant lacking the LLO toxin (Δ*hly*). The representative immunoblots in Figure 5D show that the WT bacteria induced dephosphorylation in both H3 and PP1. However, infection with the Δ*hly* strain did not induce dephosphorylation. Therefore, dephosphorylation of PP1, leading to H3 dephosphorylation, is a common mechanism activated by bacteria that produce cholesterol-dependent cytolysins and is essential for H3 dephosphorylation.

Surprisingly, although infection activates PP1, which is a pleotropic enzyme, the general phosphorylation levels of the host do not seem to be altered. Indeed, we observed no significant change in the total levels of phosphorylated serine and threonine in total cell lysates upon infection (Figure S5B). Furthermore, we tested whether activated PP1 dephosphorylated non-histone substrates, such as AKT, a kinase known to be regulated by PP1 (Thayyullathil et al., 2011; Xiao et al., 2010). AKT phosphorylation at S473 was not altered during *S. pneumoniae* infection (Figure S5B). Therefore, PP1 activation by infection seems to have some degree of substrate specificity. However, we cannot rule out that other proteins besides histone H3 are dephosphorylated during infection.

H3S10 Dephosphorylation Correlates with Transcriptional Repression of Inflammatory Genes but Is Not Required

Beyond correlation with the cell cycle, H3 phosphorylation has been associated with transcriptional activation of inflammatory genes downstream of lipopolysaccharide (LPS) stimulation (Josefowicz et al., 2016). We, therefore, hypothesized that the role of H3 dephosphorylation could be to downregulate inflammatory genes during infection. To test this, we measured the expression of a panel of 26 pro-inflammatory genes after infection with WT *S. pneumoniae*, which induces H3 dephosphorylation, and a double Δ*ply*Δ*spxB* mutant, which does not. We focused on genes that were differentially regulated between WT and the Δ*ply*Δ*spxB* mutant and found seven: *CCL2*, *CCL4*, *CCL5*, *CXCL1*, *TNF*, *CSF2*, and *IL1A*. Strikingly, although infection in WT bacteria did not significantly change the level of gene expression, the double mutant increased gene expression compared with uninfected cells (Figure 6). In contrast, expression levels of a control gene, HPRT1, were not altered. These results suggest that *S.*

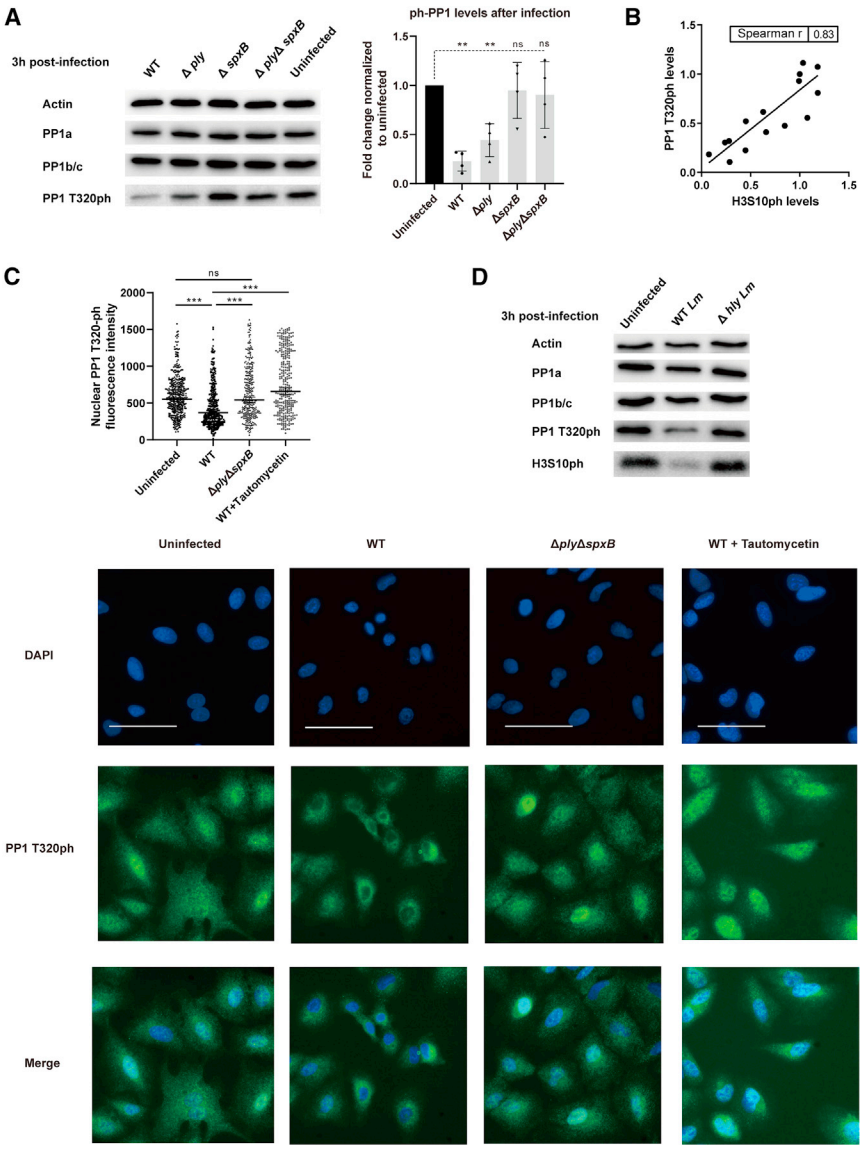

Figure 5. Bacterial Infection Induces Dephosphorylation of PP1

(A) A549 cells were infected for 3 h with WT and the indicated mutants of *S. pneumonia* strain TIGR4 (MOI = 25). A representative immunoblot (left) and a quantification (right) of four independent experiments are shown. Anti-phospho-PP1a (Thr320) antibody (Cell Signaling, 2581s) recognizes all PP1 isoforms (Shimada et al., 2010). The PP1 T320ph levels are normalized to PP1a and to the uninfected control condition. *S. pneumonia*. Error bars represent SD, and statistical significance was calculated by one-way ANOVA method (Dunnett's post hoc test, uninfected as control group). $^{**}p < 0.01$.

(B) The correlation of H3S10ph levels and PP1 T320ph levels of infected cells from four independent experiments is calculated by the nonparametric Spearman's correlation coefficient method

(C) Immunofluorescence of PP1 T320ph in A549 cells under uninfected, 3-h WT TIGR4 infection, 3-h *ΔplyΔspxB* double mutant infection, and 3-h WT infection at MOI = 25 with 3-h Tautomycetin pretreatment conditions. Size bars represent 50 μm. Quantification of nuclear PP1 T320ph fluorescence intensity from at least two independent experiments, for more than 300 cells counted for each condition.

(D) HeLa cells were infected for 3 h with the WT *Listeria* (EGD strain) and its *hly* mutant at MOI = 50. A representative immunoblot of three independent experiments is shown.

See also Figure S5.

pneumoniae actively suppressed inflammatory gene transcription in epithelial cells in a manner that is dependent on PLY and SpxB.

To determine whether *S. pneumoniae*-mediated gene suppression occurred through H3 dephosphorylation, we repeated RT-PCR analyses in the presence of the PP1 inhibitor tautomycetin. Indeed, because tautomycetin fully blocks H3 dephosphorylation, differential gene expression between WT and the Δ*ply*Δ*spxB* mutant would also be blocked in the presence of this inhibitor. However, treatment with tautomycetin did not change the transcriptional repression observed upon infection with WT bacteria for the genes tested (Figure 6). These results suggest that although H3 dephosphorylation is correlated with the repression of inflammatory genes, it is not required for it. We cannot exclude that H3 dephosphorylation could be mediating transcriptional repression of other genes, which we have not yet identified.

Blocking H3S10 Dephosphorylation through PP1 Inhibition Impairs Efficient Intracellular Infection

To determine whether PP1-mediated dephosphorylation was necessary for bacterial infection, we assessed the effect of blocking PP1 catalytic activity on infection with the chemical inhibitor tautomycetin. *In vitro S. pneumoniae* mainly remains adhered to the outside of epithelial cells (Novick et al., 2017; Weight et al., 2019). In some instances, however, it is able to invade and survive temporarily (approximately 24 h) inside epithelial cells, a mechanism that could be important for the "microinvasion" observed *in vivo* (Weight et al., 2019; Weiser et al., 2018). We first measured the effect of PP1 on bacterial adherence. We compared the number of bacteria recovered from cells treated or not treated with tautomycetin, the PP1 inhibitor. Results in Figure 7A show that there is no significant difference between the two conditions. Similar results were obtained in evaluating the number of Δ*ply*Δ*spxB* mutant bacteria in the presence or absence of tautomycetin (Figure 7A). We also evaluated the number of intracellular bacteria at 4 and 6 h after infection. Strikingly, upon inhibition of PP1 a slight, but significant decrease in the number of recovered intracellular bacteria was observed at both time points (Figure 7B). These results would suggest that PP1 is important for intracellular bacterial

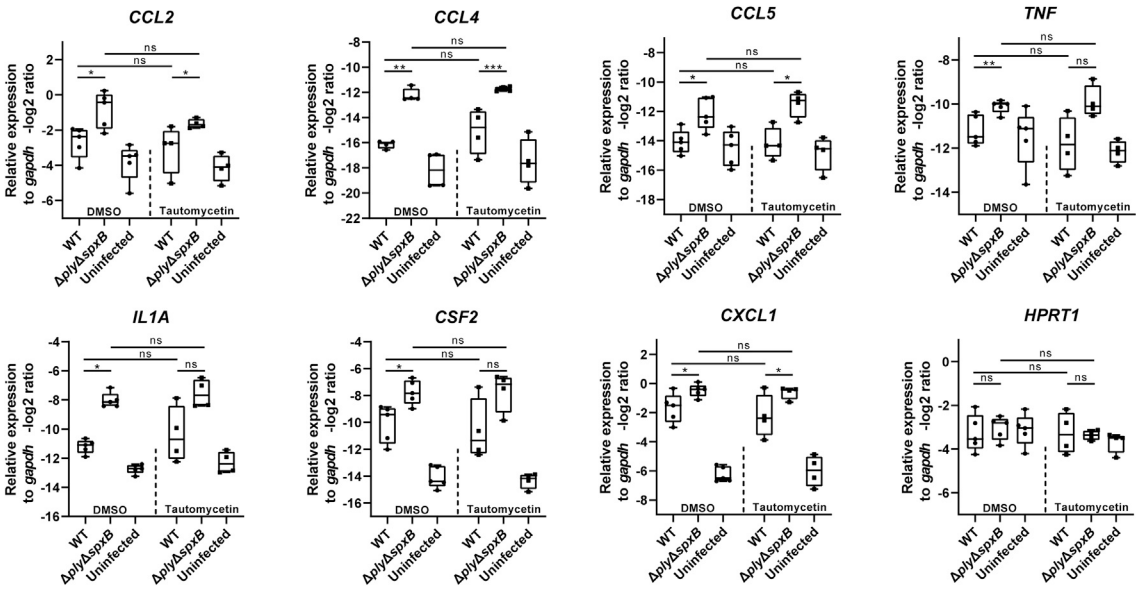

Figure 6. H3S10 Dephosphorylation Correlates with Transcriptional Repression of Inflammatory Genes but Is Not Required

Untreated cells or Tautomycetin-pretreated cells are infected by WT TIGR4 *S. pneumonia* and its *Δply ΔspxB* double mutant at MOI = 25. RNA was extracted and qRT–PCR was performed to analyze the relative expression of the indicated inflammatory genes and the housekeeping gene *hprt1*. The gene expression levels are shown as $-\log_2$ relative to the control gene *gapdh*; the results are shown as means and SD of four independent experiments. For statistical calculation, $-\log_2$-formed data are first converted to the linear form by the $2^{-\Delta CT}$ calculation, and then tested with a Student's t test. *p < 0.05, **p < 0.01, ***p < 0.001.

survival. We further tested the effect of PP1 inhibition on infection with the double Δ*ply*Δ*spxB* mutant. This mutant does not modify PP1, and no H3 dephosphorylation occurs. Interestingly, tautomycetin has no effect on intracellular survival of the Δ*ply*Δ*spxB* mutant bacteria, indicating that this inhibitor is specifically blocking PP1 activation to restrict infection (Figure 7B).

Because *L. monocytogenes*, a facultative intracellular pathogen, also activates PP1 to dephosphorylate H3, we assessed the effect of PP1 inhibition on its intracellular survival. Cells were infected with *L. monocytogenes* expressing GFP, and the fluorescence intensity of infected cells was determined by FACS analysis. Interestingly, tautomycetin-treated cells were less infected than non-treated cells, further supporting a role for PP1 in intracellular bacterial survival (Figure 7C). Therefore, bacteria triggered PP1 activation and probably the downstream H3 dephosphorylation, contributing to optimal intracellular infection of at least two unrelated bacteria.

DISCUSSION

We report here that histone H3 dephosphorylation is a common modification induced not only by pathogenic bacteria but also by a naturally colonizing bacterium, the pneumococcus. In fact, the bacterial factors involved in inducing this modification, PLY and SpxB, are common to all *S. pneumoniae* serotypes. Importantly, we demonstrate with *in vivo* samples that epithelial cells, which are the first line of defense to bacteria entering an organism, are the main cell type affected by this modification. Furthermore, the ability of bacteria to induce active PP1, and thereby H3 dephosphorylation, provides an advantage and is necessary for a productive infection.

The role of epithelial cells in a pneumococcal infection has often been overshadowed by the study of "professional" immune cells. However, more than being solely barrier cells, epithelial cells have a pivotal role in dictating pulmonary innate immune responses upon infection (Quinton and Mizgerd, 2015). In fact, selectively inhibiting canonical pathways, such as NF-κB signaling in epithelial cells, results in an impairment in neutrophil recruitment and poor activation of innate immune responses (Poynter et al., 2003). Furthermore, the epithelial barrier is responsible for the production of antibacterial components, such as defensins, chemokines, and toxic metabolic byproducts (Quinton and Mizgerd, 2015). Very recently, *S. pneumoniae* at mucosal surfaces was shown to shape epithelial transcriptomic response, including innate signaling and regulatory pathways and in inflammatory mediators, cellular metabolism, and stress response genes (Weight et al., 2019). Because histone modifications have an important role in regulating gene expression, their modification by bacteria has the potential to significantly alter host responses. A careful study of epithelial cell subtypes would define whether H3 dephosphorylation is found in epithelial progenitor cells or only in specialized and terminally differentiated cells. Such studies would be important to determine whether cells experiencing H3 dephosphorylation are turned over or are maintained beyond the presence of bacteria. Our findings that pneumococci modify host histones through active post-translational modification of a host phosphatase, which gives a growth advantage to bacteria, have far-reaching implications for both virulent and colonizing serotypes.

Cell intoxication by CDCs, including PLY, results in characteristic responses, which are the hallmarks of membrane damage, including ion fluxes, loss of cytoplasm, and host-cell death

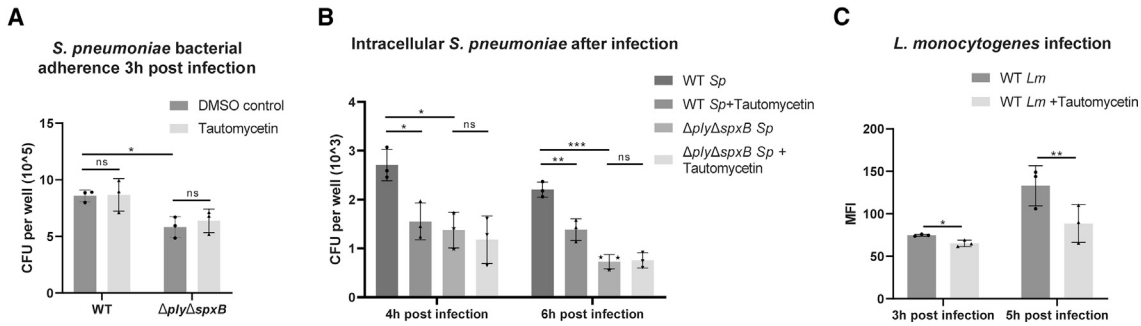

Figure 7. H3S10 Dephosphorylation Is Necessary for Efficient Bacterial Infection

(A and B) WT *S. pneumonia* (R6) and its *ΔplyΔspxB* double mutant were incubated with A549 epithelial cells at MOI = 50 and assayed for either bacterial adherence (A) or intracellular bacteria (B). The results are means ± SD from three independent experiments and statistical significance was calculated by the one-way ANOVA method (Turkey post hoc test). *p < 0.05, **p < 0.01, ***p < 0.001.

(C) Caco2 cells were infected with *L. monocytogenes* expressing GFP for the indicated times. Intracellular bacteria were detected by FACS analysis, and the mean fluorescence of intensity (MFI) was calculated. Results are means ± SD over three independent experiments. In each experiment, the ratio between the inhibitor group and the untreated control group was calculated, and the statistical significance was analyzed by the Student's t test method. *p < 0.05, **p < 0.01.

(Cassidy and O'Riordan, 2013). However, at sublethal doses, membrane repair and cell signaling are also important features. Under the conditions used in this study, we did not observe a significant amount of cytotoxicity to host cells, as determined by normal cellular morphology (Figure 1) and unaltered cell cycles upon infection (Figure S1). In agreement with these findings, *in vivo* infections with TIGR4 did not induce noticeable epithelial barrier damage and an influx of inflammatory cells. Therefore, H3 dephosphorylation is most likely not linked to *S. pneumoniae*-induced cell death.

H3S10 phosphorylation is the most common histone modification linked with bacterial infection. The activation of both NF-κB and MAPKs, which are the major host-cell response pathways to infection, leads to H3S10 phosphorylation and associated histone acetylation, resulting in transcriptional activation of target genes (Drobic et al., 2010; Yamamoto et al., 2003). Several bacterial pathogens have developed strategies to prevent H3S10 phosphorylation by disrupting pro-inflammatory kinase signaling pathways, such as lethal toxin (LT) from *Bacillus anthracis* and type III secretion-system effector OspF from *Shigella flexneri*. Both inactivate MAPKs during infection and subsequently abrogate histone H3S10 phosphorylation, which correlates with repressing inflammatory genes (Arbibe et al., 2007; Raymond et al., 2009). However, bacteria-producing CDC toxins are the only ones, to our knowledge, to induce dephosphorylation, rather than block phosphorylation, which implies that the basal levels of modified histones are changed. In addition to CDC toxins, we show that production of H_2O_2 by *S. pneumoniae* amplifies the observed dephosphorylation. Interestingly, SpxB was shown to affect the level of PLY release and epithelial cell-pore formation, indicating that the two proteins share a close link, even though the mechanism is unknown (Bryant et al., 2016). These observations could explain the phenotype of the *ΔspxB* mutant, which displays levels of H3 phosphorylation similar to the double *ΔspxBΔply* mutant and to uninfected cells. The production of H_2O_2, a freely diffusible molecule, as a metabolic byproduct has been reported for several other bacterial species, including both opportunistic pathogens, such as streptococci, probiotic or commensal enterococci, and lactobacilli (Hertzberger et al., 2014). Therefore, all H_2O_2-producing bacteria have the potential to induce H3 dephosphorylation and alter host-cell responses.

Previous attempts to link H3 dephosphorylation with a cellular effect resulted in correlative studies. We previously correlated that modification with a loss of expression of a subset of host genes (Hamon et al., 2007). However, to establish a cause-and-effect link, inhibiting H3 dephosphorylation is necessary and is only possible through inhibition of the enzyme responsible for the modification. We report here that the chemical inhibitor tautomycetin blocks H3 dephosphorylation, whereas previous attempts to identify such an inhibitor failed (Hamon et al., 2007). This important step allows us to determine that, during infection with *S. pneumoniae*, PP1-mediated H3S10 dephosphorylation is not necessary for the difference in expression of inflammatory genes between WT and mutant strains. Because H3 phosphorylation is tightly linked to transcriptional regulation (Mahadevan et al., 1991; Saccani et al., 2002; Sawicka et al., 2014), we hypothesize that *S. pneumoniae* infection may alter the expression of unidentified genes controlled by basal H3S10 phosphorylation in epithelial cells. Further studies would be necessary to identify the genes involved.

The protein phosphatase PP1 is a major protein serine/threonine phosphatase in eukaryotic cells (Peti et al., 2013). PP1 has been shown to target phosphorylated H3S10 mainly after mitosis, when H3S10 become dephosphorylated (Wu et al., 2009). The activity of PP1 is regulated through phosphorylation of T320, which is an inhibitory modification probably masking the PP1 active site and blocking PP1 substrates accessibility (Hou et al., 2013). A previous report suggested that ultraviolet irradiation induced dephosphorylation of PP1, leading to its activation and triggering subsequent histone H3T11 dephosphorylation (Shimada et al., 2010). Our data highlight that bacterial infection is able to activate PP1 through dephosphorylation, a mechanism used for its own benefit. Notably, the pathways regulated by the PP1-H3 dephosphorylation axis are conserved between at least two Gram-positive bacteria, *L. monocytogenes*

and *S. pneumoniae*, and are required for efficient intracellular infection in both models. Given the pleotropic role of PP1, we cannot fully rule out that activation of PP1 during infection dephosphorylates other factors besides histone H3. This would imply that the role of PP1 in promoting intracellular infection could involve other hosts signaling pathways. However, our data show that general dephosphorylation upon infection does not occur and that tautomycetin-mediated impairment of infection only occurs with WT bacteria, not mutant strains. Although the effect of PP1-H3 dephosphorylation on bacterial infection is slight, our findings do validate a concept that targeting host chromatin-modifying enzymes alters bacterial infection. Therefore, our study characterizes and extends the knowledge on a conserved mechanism of host subversion aimed at downplaying host response to invading bacteria.

STAR★METHODS

Detailed methods are provided in the online version of this paper and include the following:

- KEY RESOURCES TABLE
- LEAD CONTACT AND MATERIALS AVAILABILITY
- EXPERIMENTAL MODEL AND SUBJECT DETAILS
  - Bacterial culture and cell infections
  - Cell Culture
  - Mouse Husbandry
- METHODS DETAILS
  - Use of chemical and biological and reagents
  - Construction of S. pneumoniae mutants
  - *In vivo* infections
  - Cell synchronization and cell cycle analysis
  - FACS Analyses
  - Transfection of siRNA
  - Immunofluorescence
  - Western blot analyses
  - RNA extraction and Quantitative PCR analyses
- QUANTIFICATION AND STATISTICAL ANALYSIS
- DATA AND CODE AVAILABILITY

SUPPLEMENTAL INFORMATION

Supplemental Information can be found online at https://doi.org/10.1016/j.celrep.2020.02.116.

ACKNOWLEDGMENTS

Work in the M.A.H. laboratory received financial support from Institut Pasteur and the National Research Agency (ANR-EPIBACTIN). W.D. is part of the Pasteur-Paris University (PPU) International PhD Program, a project which has received funding from the European Union's Horizon 2020 research and innovation programme under the Marie Sklodowska-Curie grant agreement 665807. W.D. is supported by the EUR G.E.N.E. (reference ANR-17-EURE-0013) and is part of the Université de Paris IdEx ANR-18-IDEX-0001 funded by the French government through its "Investments for the Future" program. M.C. is supported by the Pasteur Foundation Fellowship. M.J.G.E. is supported by a fellowship from the French Government's Investissement d'Avenir program, the Laboratoire d'Excellence "Integrative Biology of Emerging Infectious Diseases" (ANR-10-LABX-62-IBEID). We would like to thank Dr. Timothy Mitchell for donating PLY toxin, and Dr. Patrick Trieu-Cuot, Dr. Thomas Kohler, Dr. Mustapha Si-Tahar, Dr. Emmanuelle Varon, and Dr. Birgitta Henriques for providing strains used in this study.

AUTHOR CONTRIBUTIONS

Conceptualization, W.D. and M.A.H.; Methodology, W.D. and M.A.H; Investigation, W.D., O.R., C.C., M.C., and M.J.G.E.; Writing – Original Draft, W.D. and M.A.H.; Writing – Review & Editing, W.D., O.R., C.C., M.C., M.J.G.E., and M.A.H.; Funding Acquisition, M.A.H.; Supervision, M.A.H.; Project Administration, M.A.H.

DECLARATION OF INTERESTS

The authors declare no competing interests.

Received: September 24, 2019
Revised: January 15, 2020
Accepted: February 21, 2020
Published: March 24, 2020

REFERENCES

Arbibe, L., Kim, D.W., Batsche, E., Pedron, T., Mateescu, B., Muchardt, C., Parsot, C., and Sansonetti, P.J. (2007). An injected bacterial effector targets chromatin access for transcription factor NF-κB to alter transcription of host genes involved in immune responses. Nat. Immunol. *8*, 47–56.

Bierne, H., Hamon, M., and Cossart, P. (2012). Epigenetics and bacterial infections. Cold Spring Harb. Perspect. Med. *2*, a010272.

Bostock, C.J., Prescott, D.M., and Kirkpatrick, J.B. (1971). An evaluation of the double thymidine block for synchronizing mammalian cells at the G1-S border. Exp. Cell Res. *68*, 163–168.

Bricker, A.L., and Camilli, A. (1999). Transformation of a type 4 encapsulated strain of *Streptococcus pneumoniae*. FEMS Microbiol. Lett. *172*, 131–135.

Bryant, J.C., Dabbs, R.C., Oswalt, K.L., Brown, L.R., Rosch, J.W., Seo, K.S., Donaldson, J.R., McDaniel, L.S., and Thornton, J.A. (2016). Pyruvate oxidase of *Streptococcus pneumoniae* contributes to pneumolysin release. BMC Microbiol. *16*, 271.

Cassidy, S.K.B., and O'Riordan, M.X.D. (2013). More than a pore: the cellular response to cholesterol-dependent cytolysins. Toxins (Basel) *5*, 618–636.

Dortet, L., Lombardi, C., Cretin, F., Dessen, A., and Filloux, A. (2018). Pore-forming activity of the *Pseudomonas aeruginosa* type III secretion system translocon alters the host epigenome. Nat. Microbiol. *3*, 378–386.

Drobic, B., Pérez-Cadahía, B., Yu, J., Kung, S.K.P., and Davie, J.R. (2010). Promoter chromatin remodeling of immediate-early genes is mediated through H3 phosphorylation at either serine 28 or 10 by the MSK1 multi-protein complex. Nucleic Acids Res. *38*, 3196–3208.

Eskandarian, H.A., Impens, F., Nahori, M.A., Soubigou, G., Coppée, J.Y., Cossart, P., and Hamon, M.A. (2013). A role for SIRT2-dependent histone H3K18 deacetylation in bacterial infection. Science *341*, 1238858.

Geno, K.A., Gilbert, G.L., Song, J.Y., Skovsted, I.C., Klugman, K.P., Jones, C., Konradsen, H.B., and Nahm, M.H. (2015). Pneumococcal capsules and their types: past, present, and future. Clin. Microbiol. Rev. *28*, 871–899.

Hamon, M.A., and Cossart, P. (2008). Histone modifications and chromatin remodeling during bacterial infections. Cell Host Microbe *4*, 100–109.

Hamon, M.A., Batsché, E., Régnault, B., Tham, T.N., Seveau, S., Muchardt, C., and Cossart, P. (2007). Histone modifications induced by a family of bacterial toxins. Proc. Natl. Acad. Sci. USA *104*, 13467–13472.

Hertzberger, R., Arents, J., Dekker, H.L., Pridmore, R.D., Gysler, C., Kleerebezem, M., and de Mattos, M.J.T. (2014). H_2O_2 production in species of the Lactobacillus acidophilus group: a central role for a novel NADH-dependent flavin reductase. Appl. Environ. Microbiol. *80*, 2229–2239.

Hou, H., Sun, L., Siddoway, B.A., Petralia, R.S., Yang, H., Gu, H., Nairn, A.C., and Xia, H. (2013). Synaptic NMDA receptor stimulation activates PP1 by inhibiting its phosphorylation by Cdk5. J. Cell Biol. *203*, 521–535.

Jeong, M.W., Kang, T.H., Kim, W., Choi, Y.H., and Kim, K.T. (2013). Mitogen-activated protein kinase phosphatase 2 regulates histone H3 phosphorylation via interaction with vaccinia-related kinase 1. Mol. Biol. Cell *24*, 373–384.

Josefowicz, S.Z., Shimada, M., Armache, A., Li, C.H., Miller, R.M., Lin, S., Yang, A., Dill, B.D., Molina, H., Park, H.S., et al. (2016). Chromatin kinases act on transcription factors and histone tails in regulation of inducible transcription. Mol. Cell *64*, 347–361.

Kadioglu, A., Weiser, J.N., Paton, J.C., and Andrew, P.W. (2008). The role of Streptococcus pneumoniae virulence factors in host respiratory colonization and disease. Nat. Rev. Microbiol. *6*, 288–301.

Li, Y., Thompson, C.M., and Lipsitch, M. (2014). A modified Janus cassette (Sweet Janus) to improve allelic replacement efficiency by high-stringency negative selection in *Streptococcus pneumoniae*. PLoS ONE *9*, e100510.

Livak, K.J., and Schmittgen, T.D. (2001). Analysis of relative gene expression data using real-time quantitative PCR and the $2^{-\Delta\Delta\ CT}$ Method. Methods *25*, 402–408.

Mahadevan, L.C., Willis, A.C., and Barratt, M.J. (1991). Rapid histone H3 phosphorylation in response to growth factors, phorbol esters, okadaic acid, and protein synthesis inhibitors. Cell *65*, 775–783.

Malet, J.K., Cossart, P., and Ribet, D. (2017). Alteration of epithelial cell lysosomal integrity induced by bacterial cholesterol-dependent cytolysins. Cell. Microbiol. *19*, e12682.

Mehr, S., and Wood, N. (2012). *Streptococcus pneumoniae*—a review of carriage, infection, serotype replacement and vaccination. Paediatr. Respir. Rev. *13*, 258–264.

Novick, S., Shagan, M., Blau, K., Lifshitz, S., Givon-Lavi, N., Grossman, N., Bodner, L., Dagan, R., and Mizrachi Nebenzahl, Y. (2017). Adhesion and invasion of *Streptococcus pneumoniae* to primary and secondary respiratory epithelial cells. Mol. Med. Rep. *15*, 65–74.

Peti, W., Nairn, A.C., and Page, R. (2013). Structural basis for protein phosphatase 1 regulation and specificity. FEBS J. *280*, 596–611.

Poynter, M.E., Irvin, C.G., and Janssen-Heininger, Y.M.W. (2003). A prominent role for airway epithelial NF-kappa B activation in lipopolysaccharide-induced airway inflammation. J. Immunol. *170*, 6257–6265.

Quinton, L.J., and Mizgerd, J.P. (2015). Dynamics of lung defense in pneumonia: resistance, resilience, and remodeling. Annu. Rev. Physiol. *77*, 407–430.

Ramos-Montañez, S., Tsui, H.C., Wayne, K.J., Morris, J.L., Peters, L.E., Zhang, F., Kazmierczak, K.M., Sham, L.T., and Winkler, M.E. (2008). Polymorphism and regulation of the spxB (pyruvate oxidase) virulence factor gene by a CBS-HotDog domain protein (SpxR) in serotype 2 *Streptococcus pneumoniae*. Mol. Microbiol. *67*, 729–746.

Raymond, B., Batsche, E., Boutillon, F., Wu, Y.Z., Leduc, D., Balloy, V., Raoust, E., Muchardt, C., Goossens, P.L., and Touqui, L. (2009). Anthrax lethal toxin impairs IL-8 expression in epithelial cells through inhibition of histone H3 modification. PLoS Pathog. *5*, e1000359.

Saccani, S., Pantano, S., and Natoli, G. (2002). p38-Dependent marking of inflammatory genes for increased NF-κB recruitment. Nat. Immunol. *3*, 69–75.

Sawicka, A., and Seiser, C. (2012). Histone H3 phosphorylation—a versatile chromatin modification for different occasions. Biochimie *94*, 2193–2201.

Sawicka, A., Hartl, D., Goiser, M., Pusch, O., Stocsits, R.R., Tamir, I.M., Mechtler, K., and Seiser, C. (2014). H3S28 phosphorylation is a hallmark of the transcriptional response to cellular stress. Genome Res. *24*, 1808–1820.

Shimada, M., Haruta, M., Niida, H., Sawamoto, K., and Nakanishi, M. (2010). Protein phosphatase 1γ is responsible for dephosphorylation of histone H3 at Thr 11 after DNA damage. EMBO Rep. *11*, 883–889.

Thayyullathil, F., Chathoth, S., Shahin, A., Kizhakkayil, J., Hago, A., Patel, M., and Galadari, S. (2011). Protein phosphatase 1-dependent dephosphorylation of Akt is the prime signaling event in sphingosine-induced apoptosis in Jurkat cells. J. Cell. Biochem. *112*, 1138–1153.

Wahl, B., O'Brien, K.L., Greenbaum, A., Majumder, A., Liu, L., Chu, Y., Lukšić, I., Nair, H., McAllister, D.A., Campbell, H., et al. (2018). Burden of *Streptococcus pneumoniae* and *Haemophilus influenzae* type b disease in children in the era of conjugate vaccines: global, regional, and national estimates for 2000-15. Lancet Glob. Health *6*, e744–e757.

Weight, C.M., Venturini, C., Pojar, S., Jochems, S.P., Reiné, J., Nikolaou, E., Solórzano, C., Noursadeghi, M., Brown, J.S., Ferreira, D.M., and Heyderman, R.S. (2019). Microinvasion by *Streptococcus pneumoniae* induces epithelial innate immunity during colonisation at the human mucosal surface. Nat. Commun. *10*, 3060.

Weiser, J.N., Ferreira, D.M., and Paton, J.C. (2018). *Streptococcus pneumoniae*: transmission, colonization and invasion. Nat. Rev. Microbiol. *16*, 355–367.

Wu, J.Q., Guo, J.Y., Tang, W., Yang, C.S., Freel, C.D., Chen, C., Nairn, A.C., and Kornbluth, S. (2009). PP1-mediated dephosphorylation of phosphoproteins at mitotic exit is controlled by inhibitor-1 and PP1 phosphorylation. Nat. Cell Biol. *11*, 644–651.

Xiao, L., Gong, L.L., Yuan, D., Deng, M., Zeng, X.M., Chen, L.L., Zhang, L., Yan, Q., Liu, J.P., Hu, X.H., et al. (2010). Protein phosphatase-1 regulates Akt1 signal transduction pathway to control gene expression, cell survival and differentiation. Cell Death Differ. *17*, 1448–1462.

Yamamoto, Y., Verma, U.N., Prajapati, S., Kwak, Y.T., and Gaynor, R.B. (2003). Histone H3 phosphorylation by IKK-α is critical for cytokine-induced gene expression. Nature *423*, 655–659.

STAR★METHODS

KEY RESOURCES TABLE

REAGENT or RESOURCE	SOURCE	IDENTIFIER
Antibodies		
anti-actin	Sigma	Cat# A5441; RRID: AB_476744
anti-H3S10ph	Millipore	Cat# MC463; RRID: AB_1163440
anti-H3	AbCam	Cat# ab1791; RRID: AB_302613
anti-H3T3ph	AbCam	Cat# ab78531; RRID: AB_1566301
anti-H3T6ph	AbCam	Cat# ab222768; RRID: AB_2820248
anti-H3T11ph	AbCam	Cat# ab5168; RRID: AB_304759
anti-H3S28ph	AbCam	Cat# ab5169; RRID: AB_304760
anti-PP1a	Santa Cruz	Cat# sc-7482; RRID: AB_628177
anti-phospho-PP1a (Thr320)	Cell Signaling	Cat# 2581S; RRID: AB_330823
anti-PP1b	Millipore	Cat# 07-1217; RRID: AB_11214026
goat anti-rabbit AF647	Invitrogen	Cat# A27040; RRID: AB_2536101
anti-AKT	Cell Signaling	Cat# 2920S; RRID: AB_1147620
anti-phospho-AKT-S473	Cell Signaling	Cat# 9271S; RRID: AB_329825
anti-phospho-(Ser/Thr) Phe	Cell Signaling	Cat# 9631S; RRID: AB_330308
anti-CD326	Miltenyi Biotec	Cat# 130-117-863; RRID: AB_2728051
anti-CD31	Miltenyi Biotec	Cat# 130-111-540; RRID: AB_2657296
anti-CD45	Miltenyi Biotec	Cat# 130-110-797; RRID: AB_2658218
Bacterial and Virus Strains		
L. monocytogenes EGD	Prof. P. Cossart	N/A
L. monocytogenes EGD expressing GFP	Prof. P. Cossart	N/A
S. pneumoniae strains, See Table S2	Multiple Institutions	N/A
Chemicals, Peptides, and Recombinant Proteins		
Tautomycetin	Tocris Bioscience	119757-73-2
Okadaic acid	Sigma	N0636
Hydrogen peroxide	Sigma	7722-84-1
PLY	Dr T. Mitchell	N/A
PLY W436A	Dr T. Mitchell	N/A
LLO	Prof. Cossart	N/A
Critical Commercial Assays		
Pierce Peroxide Assay Reagent	ThermoFisher	23281
iScript cDNA Synthesis Kit	Bio-Rad	1708890
Experimental Models: Cell Lines		
A549	ATCC	CCL-185
BEAS-2B	ATCC	CRL-9609
CaCO2	ATCC	HTB-37
HeLa	ATCC	CCL-2
Experimental Models: Organisms/Strains		
Mouse C57BL/6J	Janvier Laboratory	N/A
Oligonucleotides		
Primers for mutant construction, See Table S1	This study	N/A
Primers for qRT-PCR, See Table S3	This study	N/A
Software and Algorithms		
Flow Jo-v10	Flow Jo, LLC	https://www.flowjo.com
Prism	GraphPad Software	https://www.graphpad.com

LEAD CONTACT AND MATERIALS AVAILABILITY

Further information and requests for resources and reagents should be directed to and will be fulfilled by the Lead Contact, Melanie HAMON (melanie.hamon@pasteur.fr). All unique/stable reagents generated in this study are available from the Lead Contact with a completed Materials Transfer Agreement.

EXPERIMENTAL MODEL AND SUBJECT DETAILS

Bacterial culture and cell infections

All *S. pneumoniae* strains used in this study are listed in Table S1. *S. pneumoniae* strains were grown in Todd Hewitt broth (Bacto, BD, USA) supplemented with 50 mm HEPES at 37°C with 5% CO2 until the optical density at 600 nm = 0.6. *L. monocytogenes* strains were grown in brain-heart infusion medium (Difco, BD, USA) at 37°C with 5% CO2 until the optical density at 600 nm = 1. Bacteria were washed twice with PBS and diluted in serum-low cell culture medium. For *S. pneumoniae* strains, a multiplicity of infection (MOI) of 50:1 for R6 and a MOI of 25:1 for TIGR4 were used unless otherwise indicated. After 3h of *S. pneumoniae* infection, cells were washed with PBS for 3 times, and then either collected for future process, or cultured in medium with penicillin (10 μg /ml) and gentamicin (100 μg /ml) for later time points. For *L. monocytogenes* strains, which are described previously (Eskandarian et al., 2013; Hamon et al., 2007), a multiplicity of infection (MOI) of 50:1 was used. After 1h of Listeria infection, cells were washed with PBS 3 times, and cultured in medium with 10 μg/ml gentamycin to carry out Listeria infection for late time points.

The adherence and intracellular assays of *S. pneumoniae* were performed using A549 cells. A total of 5 × 10^6 R6 pneumococci were added to 24-well tissue culture plates containing 1 × 10^5 cells each well. After 3h infection, cells were washed 3 times with PBS to remove the unattached bacteria. To determine the amount of adherent pneumococci, PBS washed cells were lysed using sterile ddH2O. Lysates and its serial dilutions were plated on Columbia blood agar plates (43059, BIOMERIEUX) overnight at 37°C with 5% CO2, and the colony forming units (CFUs) were counted as bacteria adherence. To determine the amount of intercellular pneumococci, PBS washed cells were cultured in in medium with penicillin (10 μg /ml) and gentamicin (100 μg /ml) to kill extracellular bacteria. Sterile ddH2O was added at 4h time point after infection (namely 1h after PBS washing) or 6h time point after infection. Lysates and its serial dilutions were plated on Columbia blood agar plates overnight at 37°C with 5% CO2, and the colony forming units (CFUs) were counted as intercellular bacteria.

Cell Culture

The human alveolar epithelial cell line A549 (ATCC CCL-185) cells were cultured in F-12K culture medium supplemented with 10% fetal calf serum (FCS) and 1% glutamine. The human bronchial epithelial cell line BEAS-2B (ATCC CRL-9609) cells were cultured in DMEM culture medium supplemented with 10% FCS and 1% glutamine. The human cervical carcinoma epithelial cell line HeLa (ATCC CCL-2) cells and human colon carcinoma cell line CaCO2 (ATCC HTB-37) cells were cultured in MEM culture medium supplemented with 1% glutamine, 1 mM sodium pyruvate (GIBCO), 0.1 mM nonessential amino acid solution (GIBCO), and 10% (HeLa) or 20% ($CaCO_2$) FCS. Cells were seeded in 6-well or 24-well plates 2 days before infection. When cells were grown to semi-confluence (24h time point), they were serum-starved (0.25% FCS) for 24h before use in experiments.

Mouse Husbandry

All protocols for animal experiments were reviewed and approved by the CETEA (Comité d'Ethique pour l'Expérimentation Animale - Ethics Committee for Animal Experimentation) of the Institut Pasteur under approval number Dap170005 and were performed in accordance with national laws and institutional guidelines for animal care and use. Wild-type C57BL/6 female 8-9 week old mice purchased from Janvier Labs (France) and allowed a minimum of 7 day to acclimatize before any infections were carried out.

METHODS DETAILS

Use of chemical and biological and reagents

For experiments involving chemical inhibitors, cells were pretreated for 3h before infection with Tautomycetin (0.8 μM, Tocris Bioscience, 119757-73-2) or Okadaic acid (0.1 μM, Sigma, N0636). Hydrogen peroxide (Sigma, 7722-84-1) was added to the cells for 1h at indicated concentrations. Purified PLY and LLO were obtained as described previously (Hamon et al., 2007). Cells were treated with 6 nM LLO or 6 nM PLY for 20 or 30 min.

Construction of S. pneumoniae mutants

All primers used in construction of *S. pneumoniae* mutants are listed in Table S2. Mutants of *S. pneumoniae* were generated by transforming donor DNA into pneumococci using competence stimulating peptide (CSP) as described previously (Bricker and Camilli, 1999). To create a deletion allele with selection marker, antibiotic-resistance cassettes were fused with the upstream and

downstream flanking regions of target genes by overlapping PCR. Specifically, *ply* gene was replaced by with *erm* cassette in Δ*ply* mutant; *lytA* gene was replaced by with *erm* cassette in Δ*lytA* mutant; in Δ*spxB* mutant, *spxB* gene was replaced by *kan+sacB* (KS) cassette, which is a cassette amplified from Sweet Janus cassette (Li et al., 2014). The KS cassette permits allelic replacement or marker-free knock in through sequential positive and negative selection. Therefore, we constructed *in situ* complement strains using KS cassette. Briefly, using kanamycin-resistance positive selection, targeted sequence was replaced by KS cassette in chromosome. Using sucrose sensitivity negative selection, KS cassette was further replaced by either wild-type genes or genes carrying point mutation. Point mutation was also created by overlapping PCR.

In vivo infections

In vivo infections were performed by intranasal injection of 5 × 10^5 bacteria per mouse. Lungs were collected after 20h from infection and digested using the Lung Dissociaton Kit according to the manufacturer's instructions (Miltenyi Biotec) plus added Dispase II at 0,1U/ml (Roche). Briefly, lungs were instilled with 1ml dispase solution through the trachea before adding them to C Tubes and being digested on Octo Dissociator (Milteny Biotec). Single cell suspensions were filtered on 70um strainer before being stained to identify lung epithelial cells (CD45-CD31-CD326+). Cell were further permeabilized with Transcription Factor Staining Buffer Set (eBioscience) and stained for H3S10ph followed by secondary. Data was acquired on a MACSQuant cytometer (Milteny Biotec).

Cell synchronization and cell cycle analysis

Cells were synchronized by a thymidine block as described (Bostock et al., 1971). For cell cycle distribution, cells were detached in PBS and fixed in 70% ethanol for 1h at −20°C. Cells were washed and re-suspended in PBS containing 10 μg/ml of propidium iodide and 100 μg/ml of RNase (DNase free).

FACS Analyses

Cells infected with GFP-expressing *L. monocytogenes*, cells stained with propidium iodide, and cells from lung of infected mice and stained with antibodies, were analyzed on a FACSCalibur. Data was analyzed using the FlowJo software.

Transfection of siRNA

Lipofectamine 2000 (Invitrogen, 11-668-019) was used to introduce interference RNA into A549 cells. Pan PP1 siRNA (Santa Cruz, sc-43545) was transiently transfected (25 nM final concentration in well) to knockdown all isoforms of PP1. Scramble siRNA (On-TARGETplus SMARTpool) was transiently transfected as control. Cells were assayed 48h after siRNA transfection.

Immunofluorescence

Cells were grown on glass cover slides. After infection, cells were washed 3 times with PBS and fixed in 4% paraformaldehyde for 10 min at room temperature. After 3 washes, cells were permeabilized and blocked with 3% BSA with 0.5% Tween20 for 45 min. Immunostaining was performed with primary antibodies in 3% BSA+ 0.5% Tween20 for 90 min, and then Alexa Fluor 488 or 647 conjugated anti-immunoglobulin G (IgG) secondary antibodies in 3% BSA+ 0.5% Tween20 for 45 min.

Western blot analyses

For western blot analysis, cells were lysed using 2 × laemmli buffer (4% SDS, 20% glycerol, 200mM DTT, 0.01% bromphenol blue and 0.1 M Tris HCl, pH 6.8). Samples were sonicated for 5 s, boiled for 10 min, and then subjected to SDS-PAGE. Proteins were transferred to membrane under 2.5A/25V condition for 7min using a semidry transfer system (Trans-Blot Turbo, BIO-RAD). Transferred membranes were first blocked by TBS-Tween20 (0.1%) with 5% milk, and then incubated with primary antibodies overnight at 4°C. Membranes were washed with TBS-Tween20 (0.1%) and incubated with secondary peroxidase-conjugated anti-immunoglobulin G (IgG) antibodies for 1h at room temperature. After washing with TBS-Tween20 (0.1%), the immunoreactive bands were visualized using ECL substrate (Clarity Western ECL substrate, BIO-RAD) and imaged with a Western Blot detection system (ChemiDoc Imaging Systems, BIO-RAD). Quantification of western blots was performed using Image Lab (BIO-RAD).

RNA extraction and Quantitative PCR analyses

The mRNA was extracted from cells using an RNeasy kit (QIAGEN, 74104). DNase treatment was performed using a DNase set (QIAGEN, 79254). cDNA was then synthesized using 1 μg input RNA by BIO-RAD iScript gDNA Clear cDNA Synthesis Kit (1725035). Real-time PCR was performed using using the SYBR Green kit (iTaq Universal SYBR Green Supermix, BIO-RAD, 1725124) on a BIO-RAD CFX384. Data was obtained using BIO-RAD CFX manager. Relative gene expression analysis was performed using the $2^{-\Delta CT}$ method as described (Livak and Schmittgen, 2001). All primers used in quantitative PCR analyses are listed in Table S3.

QUANTIFICATION AND STATISTICAL ANALYSIS

The data are presented as the mean ± SD. Student's t test was used for statistical analysis when compare two groups: *, $p < 0.05$; **, $p < 0.01$; ***, $p < 0.001$. One-way ANOVA method (Dunnett's Post Hoc test when compared to control group, and Turkey Post Hoc test when compared between groups) was used for statistical analysis when compare multiple groups: *, $p < 0.05$; **, $p < 0.01$; ***, $p < 0.001$. Statistical calculations were performed using SPSS.

DATA AND CODE AVAILABILITY

This study did not generate any unique datasets or code.